EXPERIMENTAL EVALUATION OF TRANSIENT AND

STEADY-STATE CHARACTERISTICS OF A 180KW

TURBOELECTRIC-AIRCRAFT TESTRIG

By

JOSHUA DRAKE

Bachelor of Science in Electrical Engineering
Oklahoma State University
Stilwlater, Oklahoma
2020

Submitted to the Faculty of the
Graduate College of the
Oklahoma State University
in partial fulfillment of
the requirements for
the Degree of
MASTER OF SCIENCE
December, 2024

EXPERIMENTAL EVALUATION OF TRANSIENT AND STEADY-STATE CHARACTERISTICS OF A 180KW TURBOELECTRIC-AIRCRAFT TESTRIG

Thesis Approved:

Dr. Sheng

Thesis Advisor

Dr. Rouser

Dr. Third Reader

Dr. Outside Member

Name: JOSHUA DRAKE

Date of Degree: DECEMBER 2024

Title of Study: EXPERIMENTAL EVALUATION OF TRANSIENT AND STEADY-STATE CHARACTERISTICS OF A 180KW TURBOELECTRIC-AIRCRAFT TESTRIG

Major Field: ELECTRICAL ENGINEERING

Abstract:

This thesis presents the experimental results of a turboelectric-aircraft power system operating under two electrical configurations. Hybrid turboelectric power systems enable increased versitility over their singularly hydrocarbon fuel or electrically based counterparts through the combination of their advantages: energy density in the case of combustion power systems, and power density in that of electrical systems. However, much of the research pertaining to such hybrid systems has been analytical, leaving a need for implementation and experimentation to characterize operating performance. The testrig assembled to undertake this work is comprised of a Cessna-172 airframe, a modified 180kW PBS-TP100 turboprop, and the components necessary to create two electrical configurations. The first of these configurations involved the use of a low system voltage, battery augmentation, and an inductive load in the form of electic motors; whereas the second configuration used a high system voltage, a variable-resistive load, and electrical power sourced exclusively from a turbine-driven generator. Custom electronics were fabricated to aid in the control of the variable-resistive load as well as for protection of the battery. The objective of the studies conducted on this system have been to evaluate the transient and steady-state performance of turboelectric aircraft under various engine and electrical load conditions. Configuration one was tested by varying electrical throttle at maximum engine throttle, whereas configuration two was tested through repeated variation in electrical load under four fixed engine throttle points. Engine operation data was acquired from every test including output shaft torque, speed of the free and gas turbines, and combustion gas temperature, while voltage, current, and power data was recorded at different locations within the electrical systems. Tests conducted on the first configuration showed 17kW of peak electrical power: 4kW from the generator and 13kW from the battery; while 142kW of mechanical power was transfered from the turboprop. Test two demonstrated consistent waveforms accross all four turbine throttle points, with peak power output reaching 11.5kW from the generator, and XXXXkW from the engine. Observations from these tests highlight the importance of capacitance to hybrid powertrains, the forces induced on turbine engines by electric load, and functional safety considerations in the design and operation of hybrid systems. This thesis provides insight into practical implementation of turboelectric power systems for future electrified aircraft.

TABLE OF CONTENTS

LIST OF TABLES

LIST OF FIGURES

CHAPTER I

INTRODUCTION

Motivation Objectives Questions Answered

However, there is a distinct lack of practical knowledge associated with the physical construction of such systems. More public research in constructing distributed hybrid turbo-electric aircraft is needed. This paper addresses the knowledge gap by detailing the real-world implementation of electrical systems, safety systems, experimental results, and mechanical–electrical powertrain interactions. These objectives are accomplished specifically through a relatively low voltage electrical system comprised of a pulley coupled generator, battery, distributed propulsors, and requsite mechanisms to enable safe operation. A second electrical configuration was implemented into the Cessna test rig [9]to observe the transient performance of the mechainical elements of a turboelectic powertrain.

The multifaceted nature of this work presents a unique opportunity to compare the disperate effects of two electrical configurations on the mechanical systems common to both, in addition to what has been gathered from their individual operation. Configuration one is more representative of real hybrid turboelectric aircraft by nature of its use of a battery and accompanying safety mechanisms, distributed propulsion, and full integration into an airframe. Thus, the results obtained from configuration one provides insight into the benefits afforded to hybrid turboelectric systems by the inclusion of batteries, the considerations necessarry to safely use these batteries, and the increased takeoff performance of electrically augmented aircraft. Configuration two presents a worst case scenario

All sections pertaining to configuration one are recapitulated from research originally funded by the FAA and eventually published in ASME's Journal of Engineering for Gas

Turbines and Power [6]. Similarly, sections over configuration two cover research funded by NASA. The author is pursuing publication of this work for presentation at ASME's 2025 Turboexpo Conference.

CHAPTER II

BACKGROUND

2.1   Turbine Engines

A cursory understanding of turbine engines is necessarry to contextualize this work, as their improved power to weight ratio and performance at altitude when compared to piston engines make them an ideal choice for use in hybrid electric aircraft. The following is a description of how a general jet engine with a single inlet and exhuast functions. This description corresponds to the station numbering found in 1 and is applicable to the subcategories of turbine engines discuessed later.

Figure 1: Ideal Turbojet with station numbering
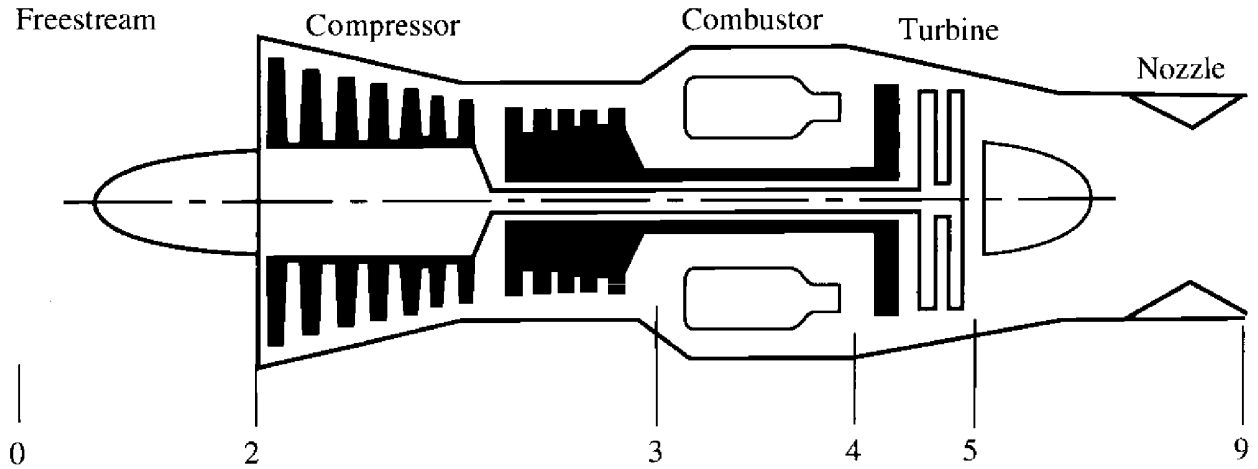
The Inlet is the first section of the gas turbine engine, denoted by station numbers 0-2, and its operation and design are described in terms of the efficiency of the compression process, the external drag of the inlet, and the mass flow into the inlet. [7] Inlet design is most heavily influenced by whether the air entering it is subsonic or supersonic. Subsonic inlet design is

simple, and typically involves selecting an operating velocity at which air compression is most efficient at the expense of performance at other velocities. Supersonic inlets must take the shockwaves endemic to supersonic flow into account for optimal performace. This is accomplished by adjusting inlet geometry to reduce flow velocity while adding as little weight to the system as possible. Variable inlet geometry will allow for increased efficiency accross many velocities.

Compressors, denoted by station numbers 2-3, increase the pressure of the flow obtained by the inlet such that the combustion and exhaust processes can be conducted more efficiently. Increasing the pressure of an initial volume of air results in the reduction of its volume, allowing for the combustion of the air/fuel mixture to occur within a smaller volume than it would otherwise. Turbine engines most commonly employ centrifugal or axial compressors. Figure 1 appropriately depicts an axial compressor in the makeup of the common turbine engine by virtue of their superiority. However, centrifugal compressors find use in smaller, less expensive engines due to their simple design. Centrifugal compressors are comprised of an impeller, which serves to increase flow velocity through rotation; a diffuser, which decreases the velocity of the flow thereby increasing its pressure; and a manifold which directs the compressed air into the combustor. Axial compressors are made of a series of stator vanes and rotor blades that are concentric to the axis of rotation. Each set of these stators and rotors is referred to as a stage. "The flow path in an axial compressor decreases in cross-sectional area in the direction of flow." [?] Each stage of the compressor results in an increase in air density. Thus, multiple stages are used in the design of high compression ratio turbine engines. Many turbines, including that which is depicted in figure 1, are equiped with dual axial compressors. Dual axial compressors allow for a more uniform loading of compressor stages, as well as for improved flexibility in the balancing between the initial and later stages.

The combustor, as illustrated in figure 1 between station numbers 3 and 4, is responsible for burning a mixture of compressed air and fuel and delivering the resulting exhaust gases to

the turbine stage at a consistent temperature. The air that enters the combustion chamber is characterized as either primary air, meaning that it mixes with fuel and burns, and secondary air, which cools the extremity of the combustion chamber as well as exhaust gases to ensure optimal temperature within the turbine. The air to fuel ratio varies from 30 to 60 parts of air to one part of fuel by weight, depending on the design and type of engine. [7] The types of combustion chambers found within tubine engines are can, which consist of multiple circular chambers arranged in a similarly circular fashion; annular, a large single chamber design around a center casing; and can-annular, a combination of the previous architectures in which can chambers are organized within an annular cavity.

The turbine section of the engine, denoted by station numbers 4 through 5, is responsible for taking the energy generated in the combustion chamber and turning it into shaft horsepower to drive the compressor stages and external loads. Almost 75 percent of the energy generated from the combustion process is required to drive the compressor alone.[7]The axial-flow turbine is similar to the axial compressor, and is likewise comprised of a series of stages of rotors and stators. However, the turbine has the opposite effect of the compressor: it turns the energy contained within flow into shaft rotation. The stage quantity of the turbine section of a given turbine engine is typically lower than that of its compressor, as the flow is expanding rather than compressing. Axial turbines are either impulse design, which maintain flow velocity across their rotor and decrease pressure across their stator, whereas reaction stages increase pressure across their rotor blades and direct flow within their stator. Most turbines use a combination of these two stage designs, and must be dual or split commensurately with the design of the compressor.

The final stage of the turbine engine, the exhaust nozzle, denoted by station numbers 5 through 9, is responsible for increasing the velocity of the exhaust gas before discharge such that ample thrust can be generated by the engine. Ideally, the exit pressure of the flow leaving the nozzle should equal ambient pressure, otherwise the engine will operate less efficiently than it is capable. Nozzles are typically either convergent, or convergent-divergent,

meaning a convergent duct followed by a divergent duct. Simple convergent ducts are used in the case where the ratio of turbine exit pressure to nozzle exit pressure is less than 2. The convergent-divergent duct is employed in instances where this nozzle pressure ratio is in excess of 2. Such ducts incorporate more sophisticated aerodynamic features and variable geometry in certain applications.[7]
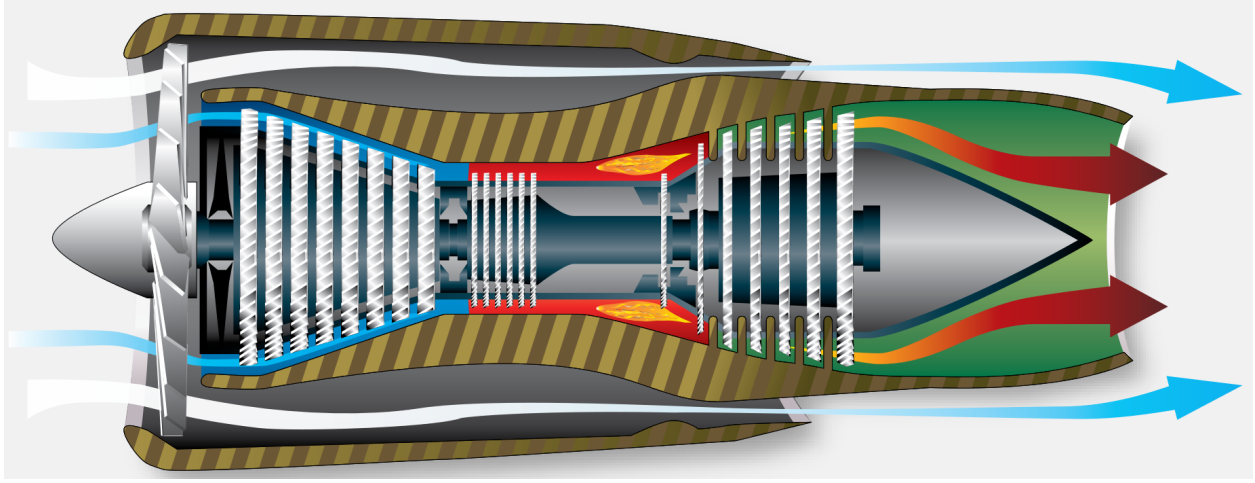

Figure 2: Turbofan Engine Cross Section

Gas turbine engines fall into four categories: turbofan, turboprop, and turboshaft, and turbojet. Turbojets make use of a propelling nozzle to create thrust by allowing the heated exhaust created by a gas turbine to expand, without extracting rotational power from the engine. [10] Turbofans make use of a front mounted fan to extract as much as 80 percent of thrust from the engine, significantly more than their turbojet counterparts. The inlets of turbofans differ from other topologies by virtue of their inlet design, as can be visualized in figure 2. The air driven by the fan will generally bypass the core, the amount of which contributes to the engine's bypass ratio. This ratio is simply the amount of flow through the engine bypass ducts over the flow through its core. The turboprop engine, that which is employed in this paper, drives a propeller through a reduction gearbox. Turboshaft style engines are most often used in helicopters, and are characterized by their transfer of power to a shaft which later connects to another implement such as a propeller transmission or
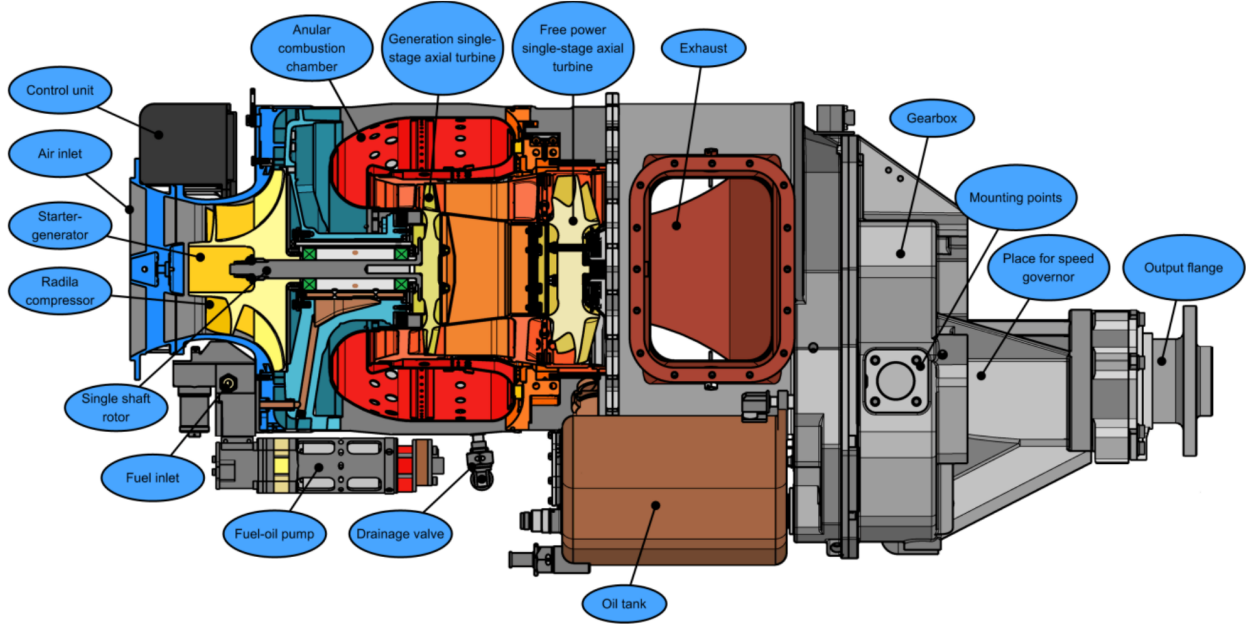
auxilary power unit. [4]

Figure 3: PBS TP100 Cutaway

2.2 Generator Theory

2.3 Battery Theory

$$I_{Battery} = \frac{V_{Battery} - V_{Supply}}{R_{Battery}} \tag{1}$$

2.4 Turboelectric Theory

NASA defines turboelectric systems as being at the least a turboshaft coupled to an electric generator, which power electric motors which then drive propellers. This configuration can be further categorized in accordance with whether the turbine engine drives a load directly. These systems, refered to as "Partial Turbo Electric" [5], employ the use of either turbofans or turboprops in addition to being coupled to electric generators. The last manner in which turboelectric systems can be categorized is with respect to their inclusion of additional power sources. For example, just as is illustrated in figure 5, systems with battery supplementation
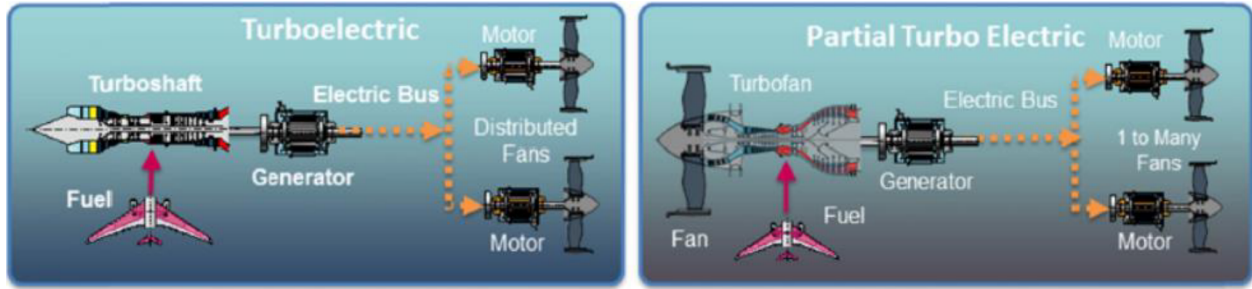
Figure 4: Turboelectric Architectures

are called "parallel," whereas those which source power exclusively from their turbine engine are "seires." [5] Both systems constructed for this research are partial by virtue of their turboprop engines. However, configuration 1 is parallel due to its inclusion of a battery, whereas configuration 2 is devoid of additional power sources and is thus series.
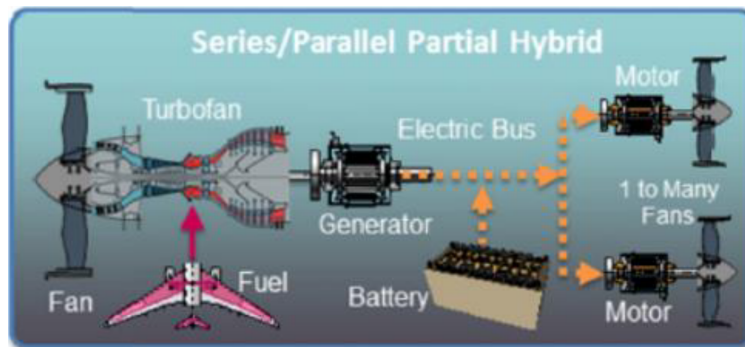

Figure 5: Parallel Turboelectric Design

2.5 Previous Work

CHAPTER III

METHODOLOGY

3.1   General Aircraft System

3.2   Configuration One

Component	Specification	Serial Number
Generator	50-kW, 27-kV,120-V Max	15412015470
Rectifier 3×	500-A, 1600-V	MDS400A1600V
Main Battery 2×	LiPo, 17000-mAh, 14S, 15C, 880.6-Wh	MA-17000-14s-Lipo-Pack
Engine Battery	24-V Lead Acid	
Contactor 2×	500-A, 900-VDC, 24-VDC Coil	LEV200A5ANA
Pre-Charge Resistor	100-Ω	
Crowbar Resistor	10-Ω 1500-W Continuous	279-TE1500B10RJ
Main Wire	6AWG Silicone Jacket Wire, 200°C, tinned	SW6A3200008F25C2
Battery/ESC Connector	500-A Max, 200°C	QS10-S
Phase Connectors	10-mm Bullet Connectors	B00CDAPJ74
ESC 2×	Flier 120-V, 500A	F-500S-A
Wing Mounted Motor 2×	50-kW, 36-kV, 120-V Max	15412015470
Wing Mounted Propeller 2×	2 Blade CF, 0.7-kg, 50×12-in, 77-lbf	

Table 1: Configuration One Power System Components

3.2.1 Data Acquisition

The turboprop engine control unit (ECU) connects to a laptop-based program. This program outputs various metrics of the engine and can be used to record data visually. Unfortunately, the controller area network bus protocol used by the engine is proprietary and the manufacturer did not provide software to record data directly. Thus, all engine data was recorded from video capture of real-time graphical read-out, and figures were created during post-processing. **Include PBS CAN Table!!!!** The main data acquisition system consists of three Arduino Megas. Two of the microcontrollers were utilized to record most of the sensor inputs. The third Arduino only measures voltage and was located inside the aircraft with the pilot. The two main boards interface with printed circuit boards serve to isolate the controllers from the high voltage of the system and filter noise. The board was designed to accommodate the numerous sensors present on the aircraft, though this paper will focus on the power data because most of the recorded data was thermistor data and not particularly interesting. All the specifics of the relevant DAQ components are listed in Table 2. The

Component	Specification	Serial Number
DAQ 3×	Arduino Mega	A000067
Current Sensor	500-A, 2%	LEM DHAB S-124
Current Sensor 2×	750-A, 2%	LEM DHAB S-133
Voltage Sensor	Arduino Mega ADC, 10-bit	A000067
ESC Controller	Variable PWM Output	B09TW3CY87
Microphone 3×	Dual Omnidirectional Microphones	DR-05V2

Table 2: Configuration One Data Acquisition Components

locations of the hall effect current sensors can be seen in the main electrical system diagram shown in **REDO Diagram!!!**. The aircraft testbed consists of 2 LEM DHAB S-133 current sensors that can read up to 750-A and are accurate to within 2% of the actual value. They are located after the generator and before the crowbar circuit. A third DHAB S-124 current

sensor was also used before the battery, and it can read up to 500-A accurately. This sensor is slightly more accurate than the S-133 because it has a smaller current rating. The amount of power expended from the battery was not expected to exceed 300-A. These three sensors allow for current in the system to be fully accounted for and monitored. The current sensors are bidirectional and so can determine the direction electrical current is flowing. All power production (battery and generator) and power utilization (battery, wings, and crowbar) can be accurately measured in real-time. A voltage divider was utilized to reduce the 120-V to a 5-V range. This scaled range was then read by the analog port on an Arduino. For the voltage sensor, a separate dedicated Arduino was used to allow for an increased response rate and ease of electrical isolation.

3.2.2 Experimental Procedure

ESC Throttle	Turboprop Throttle
Off	Step 0
Low	Step 1
Medium	Step 2
High	Step 3
Medium	Step 4
Low	Step 5

Table 3: Configuration One Test Matrix

Before hybrid-power testing commenced, the system went through a series of preliminary tests to reduce the technical risk of a full hybrid-power system test. These tests were important for informing the test matrix design. First, the turboprop engine was tested to ensure the engine was operating nominally, before adding the generator [9]. Next, a check run was performed using only the batteries, ensuring the power system and electric motors worked properly. The test confirmed that the data acquisition system and electric motors

worked correctly. Before full system testing commenced, the generator was plugged into the power system and the engine was slowly brought up to speed to find the point where the generator voltage exceeded the battery voltage. During this testing, it was discovered that the generator had a k V of 27 instead of the expected value of 23. The test procedure for the ground test rig consists of first charging and balancing the batteries. The batteries are then installed into the aircraft, with one battery connector left disconnected until just prior to the test. The aircraft strut is filled with air, the engine oil level is checked, and the brakes are checked. The aircraft is rolled out of its hanger and brought to an open field. The aircraft is then secured with a chain to the ground. The precharge circuit is then activated, and batteries are plugged into the main bus. The precharge circuit is then disabled. Two people then get into the aircraft, a pilot and a data recorder with a laptop. A third person records a video with a fire extinguisher on standby. The data recorder confirms that all sensors are working. Then the engine is started and brought to idle. Once the engine has reached operating temperature and is ready, the pilot designates the beginning of testing and brings up the throttle to the test point. The data recorder then brings up the electric motors to the respective test points. Finally, after the data have been recorded, the engine is brought down to idle and then turned off. The engine is cooled, the main power battery is disconnected, and the data are exported to the laptop hard drive. The test matrix was designed to accommodate the 27-k V value generator. If the voltage of the battery is higher than the output voltage of the generator, then no power is generated and the generator spins freely. This amounts to an all-electric configuration in practice if the generator is outputting below the battery voltage. The output voltage of the generator is around 111.1-V at the maximum power turbine shaft speed. The minimum battery voltage that was deemed safe is around 20% of the useful capacity. This meant that the cell voltage of the batteries was brought down to 3.81-V per cell. This brought the 28S battery to a total of 106.7-V, which meant that the generator would only be operating slightly above the battery voltage. The maximum voltage of the battery at 4.2-V per cell is 117.6-V. This has practical advantages

as it makes it difficult to overcharge the battery if the generator's output voltage is less than the total maximum voltage of the battery. The net effect of the 27-k V generator was that the generator voltage would only exceed the battery voltage at full throttle. This meant that the full engine throttle test point was the only engine test point of interest. The maximum charging current of the battery specified by the manufacturer is 85-A and should not be exceeded. Based on this value and the known resistance values of the batteries, Eq. (2) was used to determine that a voltage difference of 7-V between the battery and generator would be needed to exceed the maximum current rating. However, the largest value that the generator could output was 111.1-V and the minimum battery voltage was 106.7, which lead to a maximum difference of 4.3-V, which is well below 7-V. In practice, because the maximum RPM is not normally achieved under normal operation and there is a voltage drop across the rectifier the full 111.1-V, generator output will not be achieved. The test matrix in Table 3 was designed to operate at the full turboprop throttle position. The test procedure was developed to capture steady and transient data. The engine would be brought up to idle and then brought to full throttle. The low ESC throttle value was intended to be around 30-A per motor based on previous electric tests, with a medium value of around 80-A, and a high value intended to be around 150-A per motor. Both electric motors are brought up to a low value and then held for 5-s, before moving to the next value and holding it for 5-s as well. The result provided data at different relatively steady conditions, as well as the transient reaction of the electromechanical system to changes in the electrical load.

3.3   Configuration Two

3.3.1   Data Acquisition

3.3.2   Experimental Procedure

CHAPTER IV

RESULTS

4.1   Configuration One

4.1.1   Turboprop Engine Data

Figure 11 shows the power turbine shaft torque output and rotational speed throughout the test run. The impact of the power generator can be seen in the mechanical system data. The turboprop was taken to full throttle and left there for the duration of the electrical system testing. The turboprop maintains a specific shaft speed at each throttle setting and so should not change throughout the run. The decrease in RPM around the 355-s mark was caused by the load of the generator slowing it down. After 5-s, the engine control unit brought the turboprop back to the intended speed. However, it can be seen that the engine was now producing more torque at that same RPM, and thus more power. The turboprop is rated for a peak shaft speed of 2158-RPM, which was used in the design of the generator system. The peak value measured during testing was 2136-RPM. So, the generator was spinning at 2990-RPM and the design speed for the generator is 3000-RPM, so it was operating nominally. The peak power produced by the turboprop was about 150-kW. The nominal max continuous output of the engine is 160-kW, but the engine can temporarily boost to 180-kW for takeoff. This means that throughout testing, the maximum power rating of the engine was never exceeded. The engine performed well, and no otherwise unexpected phenomenon happened to the engine throughout testing.
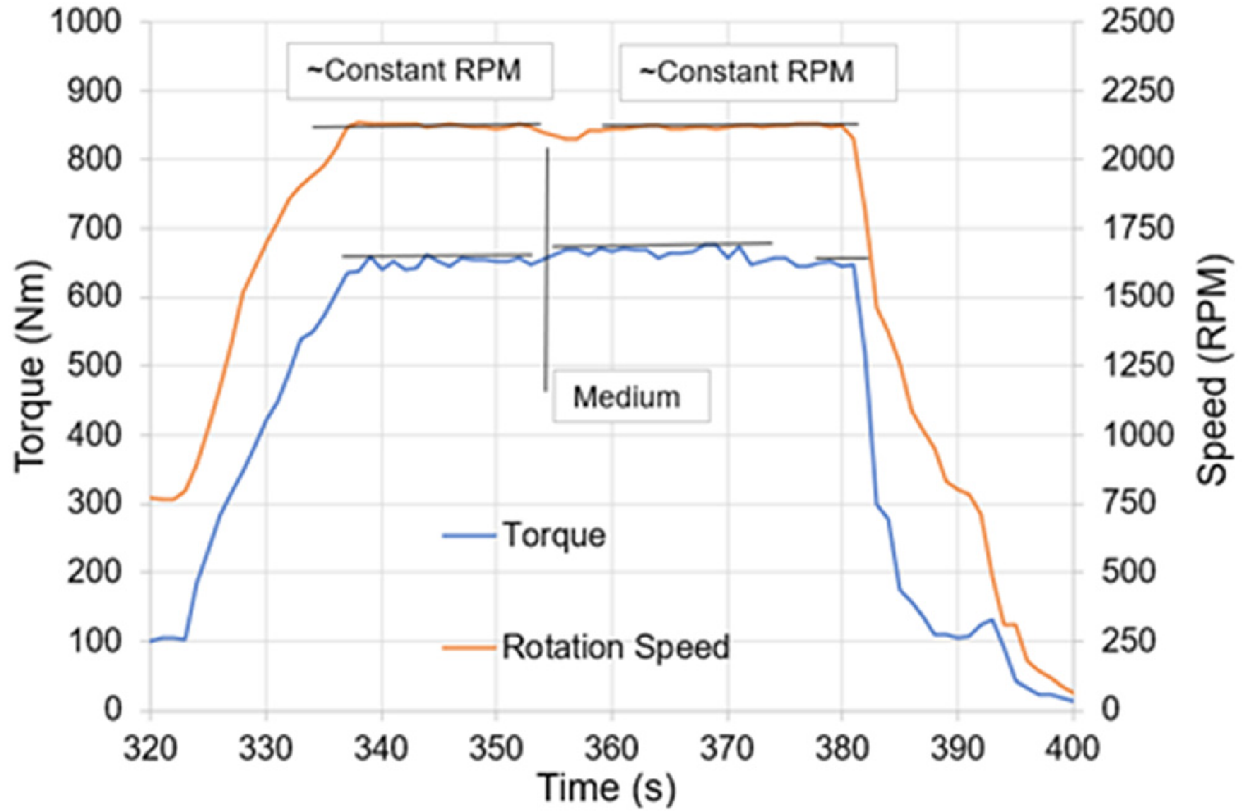
Figure 6: Turboprop Shaft Torque and Speed

4.1.2 Electrical System Performance

Figure 12 shows the voltage of the central bus and the current flow from the generator and battery. The ESC throttle positions are labeled in the figure. The voltage data contain some noise caused by the electrical output of the generator. The cause of the noise being something else, such as the vibration of the instrumentation, is unlikely because it only appears when the generator hits the designed speed and exceeds the voltage of the battery. The Arduino and probes that measure the main bus voltage are also not located on the engine, further increasing the notion that the noise is caused by the generator creating a noisy DC signal.

Figure 13 shows the total electrical and mechanical power during the same period as Fig. 12, allowing for direct comparison. The trends for the voltage data are quite clear. The battery begins at 106.5-V and ends at 105.9-V. Under peak load at around 365-s, the mini-

15

mum operating voltage of 100-V is achieved. From left to right, the changes in ESC throttle position can be seen. Starting from the left the battery begins charging at 14.4-A. The two ESCs are then commanded to start at the expected nearly 15-A current draw, but the left ESC failed to engage properly.

Surprisingly, the medium throttle position on the right ESC was achieved by drawing 75-A, but the amount of current from the generator saw only a minor increase. Instead, the difference was almost entirely picked up by the battery. This can also be seen in the power data. There is a small bump in generator power at the ESC medium point, but the power decreases slightly and is picked up by the battery. The mechanical data show a drop in rotational speed at about the same time the medium throttle point was engaged. Whenever the load was increased, it slowed down the rotational speed (and thus voltage) of the generator preventing it from picking up the difference. The generator was slowed down from the near constant 2990-RPM to 2904-RPM, which would have reduced the output voltage by 3-V. Because the output voltage of the generator is so close to the battery voltage, this decrease in voltage significantly impacted the current output. The battery responded to the increased load almost instantly but based on the power/RPM data, it took 5-s for the turboprop ECU to adequately react to the increase in mechanical load.

Once the high ESC throttle position was reached, a significant amount of current 150-A total was discharged. The voltage then dropped by several volts and the amount of current from the generator increased significantly to its maximum of 39-A. At this point, around 4-kW was being extracted from the turboprop using the generator, while about 13-kW of power came from the battery.

Afterward, the second medium throttle position was hit. The total current was 40-A compared to the previous 75-A. The reason for the significant difference may have been an error made by the operator, who may have missed the target ESC throttle positions. The power data, however, provides evidence that the total power output of the propeller was continuously decreasing despite the operator holding the throttle steady for each position.

The simple explanation may be that the inertia of the propeller and electric motor is quite large. The electric motor did not require as much power because it was slowing down instead of speeding up. The final observation is that the resting current output of the generator recharging the battery is slightly higher than at the beginning of the run. This is because the voltage difference between the generator and battery increased since the battery discharged some of its power.
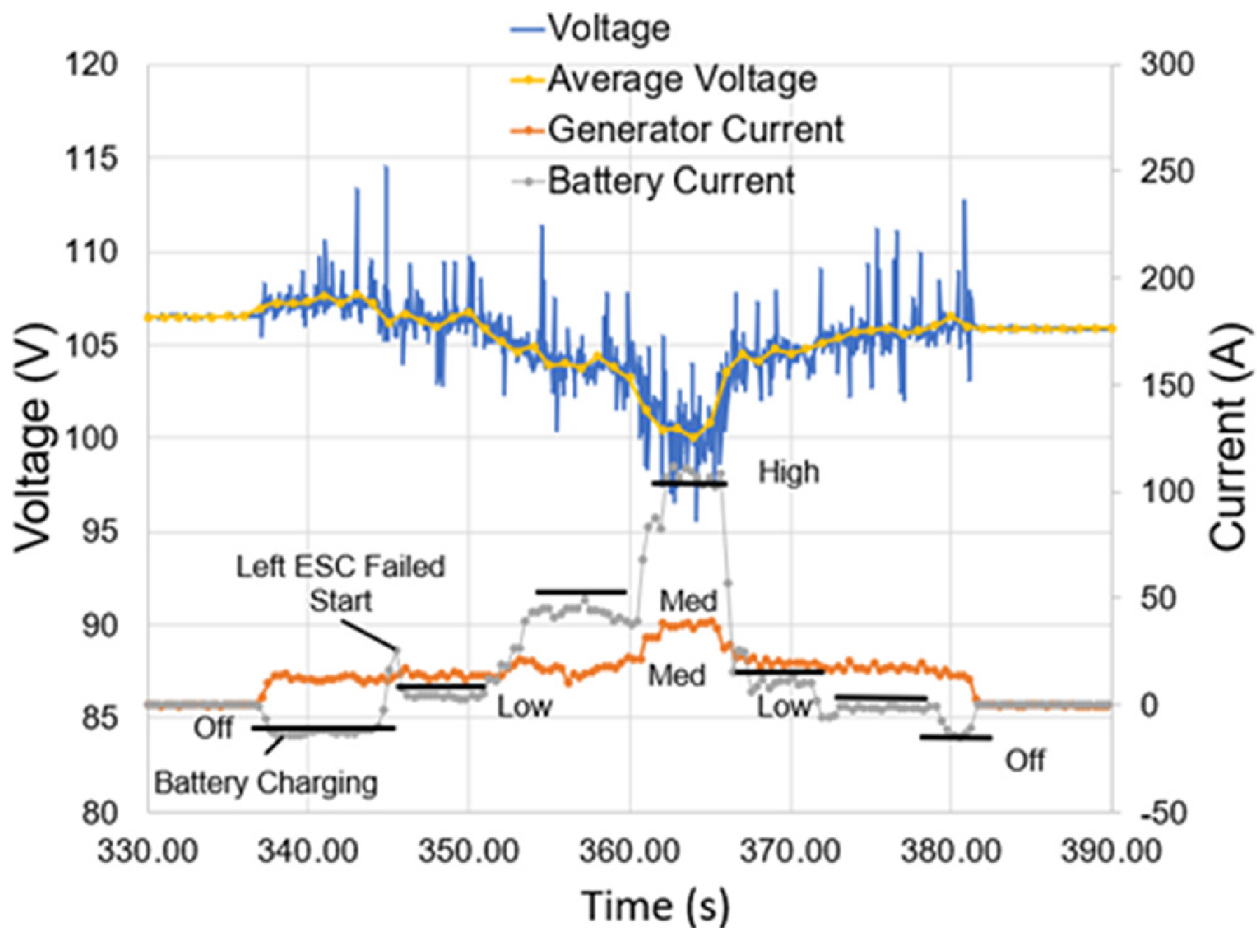

Figure 7: Voltage and Current Data

4.1.3   Electronic Speed Controller Failure

After the main test was completed, the left ESC that had failed to start properly was investigated. The ESC and electric motor had previously been successfully tested during an all-electric check-out test run. The electric motor was again tested on battery power to figure
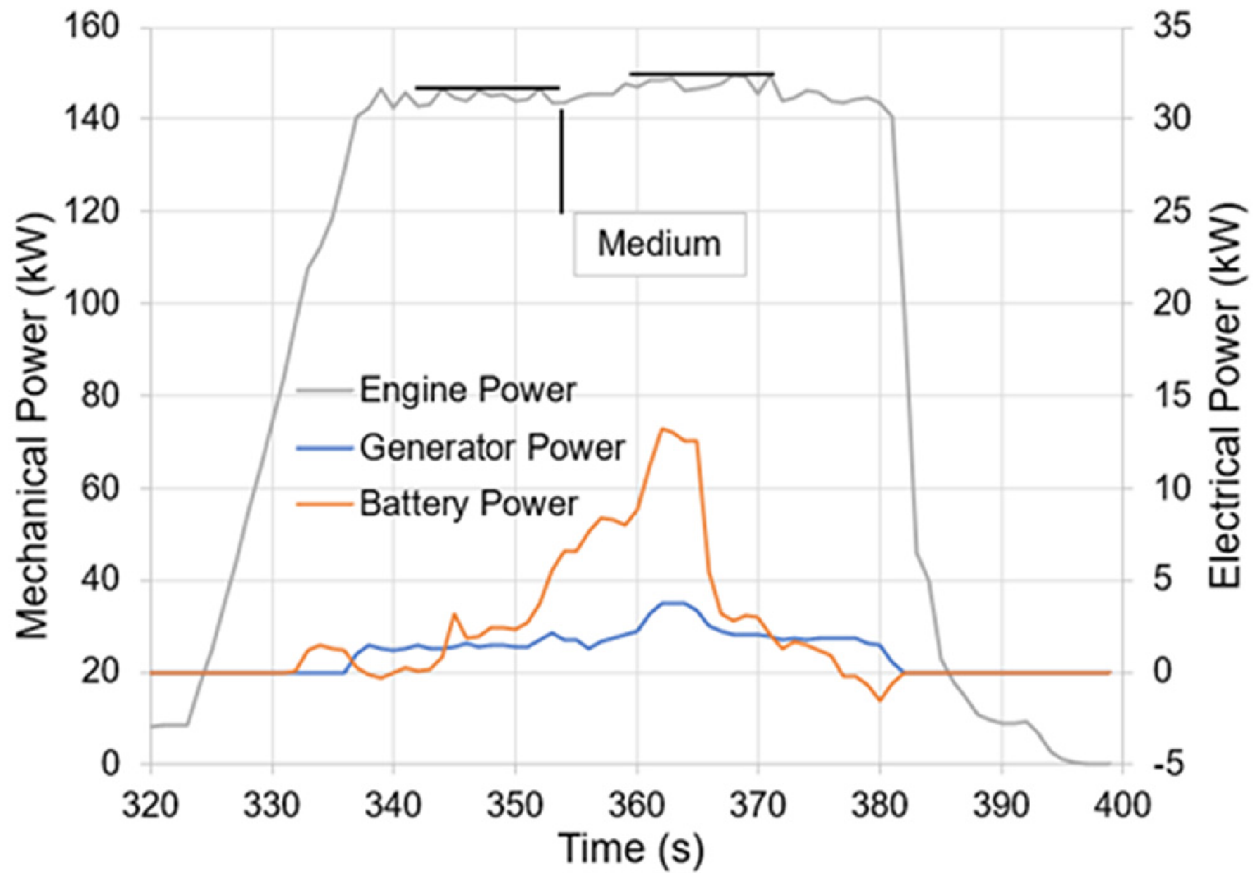
17

Figure 8: Mechanical versus Electrical Power

out what was wrong. During this attempt at starting the motor, the ESC saw a significant in-rush current as shown in Fig. 14. This caused spontaneous failure and the rupturing of the capacitors inside the ESC creating a minor fire. The current draw during failure shown in Fig. 14 is an underestimate. The sensor used to monitor the battery current maxes out slightly over 500-A, so the instantaneous maximum values may have been higher than 550-A. The electrical data during the failure were of particular interest. During previous testing, an ESC had desoldered its connection point with its main power wire, which had removed the ESC load from the main bus. In this case, the ESC shorted, causing a substantial unexpected load of 46-kW of electrical power on the central bus. This caused significant strain on the battery, whose maximum rated current was around 350-A. Had this event occurred during full system testing, then it could have damaged the turboprop engine or the battery.

The acquisition rate of the current sensor data is slow compared to the failure causing steep step changes. However, it appears that as the failed system was failing, the minimum of the oscillating current expenditure creeps up from around 20-A (at 423-s) to about 50-A (428-s). This gave rise to clear recommendations for the handling of electrical failure modes.

4.2   Configuration Two

CHAPTER V

CONCLUSION, RECOMMENDATIONS, AND FUTURE WORK

5.1   Configuration One

The experimental characterization of the electromechanical performance of the partial-hybrid turbo-electric aircraft ground test vehicle was accomplished. The peak power generated was about 4-kW, which was used to power the right-wing motor along with 13-kW of power from the battery. The total engine output was around 150-kW. The electrical power generated was significantly more than the 0.72-kW generated by the original engine alternator. Based on the performance metrics of the engine, the maximum power output and the speed of the turboprop were kept well within the nominal range.

The interdependent time response of the combined machine was interesting. The turbine engine was operating at 150-kW of shaft power whenever the generator was fully engaged at 4-kW. The battery met the required load, but the turboprop was slowed down by the generator and took almost 5-s to return to the nominal RPM value. The slow response of the turbine to such a minor adjustment in power was unexpected. The power split between the generator and the battery during the transition from low to medium throttle was also of particular interest. The current flow from the generator changed only slightly with the difference being made up by the battery. The reason for the slight change was an impact on the rotational speed of the generator and its effect on output voltage. The slowdown from the near-constant turboprop shaft speed led to a 3-V decrease in the output of the generator. Because the output voltage of the generator was so close to the battery voltage, this decrease in voltage significantly impacted the current output and prevented it from meeting

the electrical system demand. Once the turboprop rotational speed returned to normal, the generator was able to produce more current.

Additionally, a failure mode caused by a short in the left ESC was identified. The bus voltage dropped considerably from 106-V to somewhere near 40-V. The current output of the ESC reached at least 550-A and drew a minimum of 46-kW of power from the battery. The power system was able to temporarily accommodate the failure, but it highlighted that the power system needed to be able to accommodate a power failure that pulled all available electrical power in the system.

Finally, a qualitative analysis of the acoustic signature of the aircraft testbed showed there was little difference between the OASPL of the aircraft with and without the electric propeller operating. This demonstrates that the dominant noise source is likely the turboprop engine or acoustic interactions related to the turboprop engine. A cowling with acoustic dampening material could potentially change this outcome, especially since the engine in this configuration is not enclosed.

REFERENCES

[1] PBS Aerospace, *Basic technical information turboprop engine tp100*, April 2015.

[2] Cheryl L. Bowman, Ty V. Marien, and James L. Felder, *Turbo- and hybrid-electrified aircraft propulsion for commercial transport*, 2018.

[3] Johnathan Burgess, Timothy Runnels, Joshua Johnsen, Joshua Drake, and Kurt Rouser, *Experimental comparison of direct and active throttle control of a 7 kw turboelectric power system for unmanned aircraft*, Applied Sciences **11** (2021), no. 22.

[4] FAA, *Aircraft engines*, Federal Aviation Administration, 2024.

[5] Ralph Jansen, *Overview of nasa electrified aircraft propulsion activities*, NASA Glenn Research Center, 2017.

[6] Joshua Johnsen, Joshua Melvin, Joshua Drake, Muwanika Jdiobe, and Kurt Rouser, *Experimental evaluation of an electric powertrain designed for a 180-kw turboelectric aircraft ground test rig*, Journal of Engineering for Gas Turbines and Power **146** (2024).

[7] Jack Mattingly and Hans von Obain, *Elements of propulsion: Gas turbines and rockets 2nd edition*, AIAA, 2016.

[8] Joshua Melvin, *Integration and evaluation of a 180-kw turboprop engine with a turboelectric ground test rig*, Master's thesis, OKLAHOMA STATE UNIVERSITY, May 2021.

[9] Joshua Melvin and Kurt Rouser, *Development of a turboelectric ground test-rig by installation of a 180-kw turboprop onto a cessna-172*, no. 2024-0137, AIAA, 2024.

[10] NASA, *Turbojet engine*, NASA Glenn Research Center, 2017.

[11] Manuel Rendón, Carlos Sánchez, Josselyn Gallo Muñoz, and Alexandre Anzai, *Aircraft hybrid-electric propulsion: Development trends, challenges and opportunities (https://rdcu.be/cmg4u)*, Sba Controle & Automação Sociedade Brasileira de Automatica (2021).

APPENDICES

Title of Appendix (Not Numbered)

Lorem ipsum dolor sit amet, consectetur adipiscing elit. Etiam finibus venenatis dui, a accumsan dui elementum non. Suspendisse suscipit diam sed dapibus mollis. Quisque id congue nisl, auctor elementum turpis. Sed mattis at leo non rhoncus. Donec at rhoncus velit, at dignissim risus. Sed in quam a felis pulvinar bibendum a eget mi. Aliquam ac ligula nec urna pharetra interdum. Nam varius quis dui non finibus. Proin ullamcorper blandit ipsum nec feugiat.

VITA

Joshua Drake

Candidate for the Degree of

Master of Science

Thesis: EXPERIMENTAL EVALUATION OF TRANSIENT AND STEADY-STATE CHARACTERISTICS OF A 180KW TURBOELECTRIC-AIRCRAFT TESTRIG

Major Field: Electrical Engineering

Biographical:

Education:

Completed the requirements for the Master of Science in Electrical Engineering at Oklahoma State University, Stillwater, Oklahoma in 2024.

Completed the requirements for the Bachelor of Science in Electrical Engineering at Oklahoma State University, Stillwater, Oklahoma in 2020.

Experience:

Research and Design Engineer The Toro Company 2020-2023
Research and Design Engineer OAIRE Current